Analysis and Improvement of Low-Frequency Control of Speed-Sensorless AC Drive Fed by Three-Level Inverter

Jie (Jay) Chang†

Abstract - In induction machine drive without a speed sensor, the estimation of the motor flux and speed often becomes deteriorated at low speeds with low back EMF. Our analysis shows that, in addition to the state resistance variation, the estimated value of field orientation angle is often corrupted by accumulative errors from the integration of voltage variables at motor terminals that have low signal/noise ratio at low frequencies. A repetitive loop path of integration in the feedback can amplify this type of error, thus speeding up the degradation process. The control system runs into information starvation due to the loss of correct field orientation. The machine's spiral vectors are controlled only in a reduced dimension in this situation. A novel control scheme is developed to improve the control performance of motor's current, torque and speed at low frequencies. The scheme gains a full-dimensional vector control and is less sensitive to the combined effect of the error sources at the low frequencies. Experimental tests demonstrate promising performances are achievable even below 0.5 Hz.

Keywords: speed-sensorless control, performance degradation at low-speeds, motor flux estimation, accumulation of the estimation error, low signal/noise ratio

1. Introduction

Many industrial AC drives fed by PWM voltage source inverters employ open-loop volts/hertz control for a type of "general" applications, such as fans, water and sewage pumping, etc. However, this control has shown insufficient performance for many other applications. In addition to its slow torque response due to nonlinear coupling between it's flux and torque producing components [1], one of the major drawbacks is lacking of motor current regulation. Nuisance trips take place by current surges due to large load variations or starting into a spinning motor at an unknown speed.

By regulating motor currents in a synchronous rotating reference frame or a pseudo-rotating reference frame [3-4] in a speed-sensorless control [1-3, 5], improved current control can be obtained. A linear torque control is achieved by field orientation [1] approach, which decouples the control between the motor flux and torque producing current. Among various schemes [5-9], stator-flux oriented speed sensorless control offers suitability in controlling standard induction machines and relatively simple algorithm. While providing reasonable performance at high frequencies, the control performance of this scheme at low frequencies remains more to be desired. The motor current distortion becomes significant at low frequencies.

On the other hand, the thermal variation of the stator resistance has been identified for adversely affecting the control at low speeds [10]. However, there exist other error sources in a practical drive system that has significant impact on the drive control, which is to be detailed in this paper.

Upon reviewing the practical control problems, a detailed analysis of the error sources is given in Section II to IV. It further reveals that the machine spiral vectors in a conventional scheme can be controlled only in reduced dimension at low frequencies, and a structural weakness exists at this situation. A novel control scheme for speed-sensorless control is therefore discussed in Section V. The control scheme is implemented and discussed in Section V Preliminary experimental tests demonstrate improved control performance in motor current, torque and speed, even below 0.5 Hz.

2. Power Circuit of Three-Level Inverter

A three-level IGBT inverter power circuit is shown in Fig. 1. The 3-level PWM control [11] offers advantages such as: (1) ½ per-unit voltage rating of switching power device. (2) ½ dv/dt stress on the motor stator windings. (3) ½ switching frequency requirement in comparison with 2-level PWM, thus reducing the switching losses.

The control scheme includes estimation of motor flux, field orientation angle and motor speed, which will be discussed in the following sections.

This paper was received the best paper award from ICEMS 2005, which held in Nanjing, China from Sep. 27 to Sep. 29, 2005

† Corresponding Author: Florida State University, Florida, 32310, U.S.A (jchang@eng.fsu.edu)

Received November 3, 2005 ; Accepted November 18, 2005

3. Conventional Flux and Speed Estimation

The stator flux of an induction motor, λ_1, can be obtained by integration of the machine's stator back-EMF that is obtained by motor terminal voltage minus the voltage drop on the stator resistor. The stator voltages can be obtained by voltage sensing circuits that have high-impedance isolation from the high voltage source and the current signals are available from the Hall-effect current sensors.

$$\lambda_{1\alpha} = \int (V_{1\alpha} - R_1 i_{1\alpha})\, dt \tag{1}$$

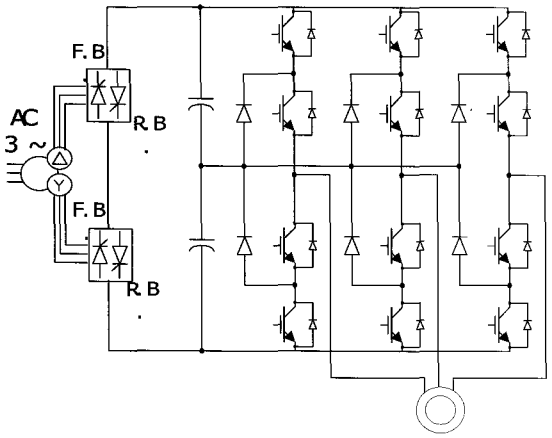

Fig. 1 Three-level PWM IGBT inverter drive

$$\lambda_{1\beta} = \int (V_{1\beta} - R_1 i_{1\beta})\, dt \tag{2}$$

The variable definitions are given in nomenclature at the end of this paper. The motor synchronous angular speed is estimated by:

$$\omega_1 = \frac{(V_{1\alpha} - R_1 i_{1\alpha})\lambda_{1\alpha} - (V_{1\beta} - R_1 i_{1\beta})\lambda_{1\beta}}{|\lambda_1|^2} \tag{3}$$

The orientation angle of the rotating reference frame can be obtained by integration of the estimated synchronous speed:

$$\varphi = \tan^{-1}\left(\frac{\lambda_{1\beta}}{\lambda_{1\alpha}}\right) = \int_0^t \omega_1\, dt \tag{4}$$

The rotor electrical angular frequency is given by

$$\omega_{re} = \omega_1 - \omega_{sl} \tag{5}$$

The motor slip angular frequency can be related to the motor primary currents by

$$\omega_{sl} = \frac{L_m}{T_2 \lambda_2} i_{1q} = \frac{1 + pT_2}{T_2} \frac{i_{1q}}{i_{1d}} \tag{6}$$

4. Analysis Of Error Sources And Control Degradation At Low Frequencie

4.1 Error Sources, Signal/Noise Ratio and Loop Effects

Although acceptable performance can be obtained by conventional sensorless control approaches at high speed for medium performance industry drive applications, the accuracy of stator flux estimation is unfortunately very limited at low frequency. This problem can be analyzed by identifying the main error contributors, examining the signal/noise ratio and investigating their effects on the drive control.

Not surprisingly, in a practical system the actual feedback flux signals are contaminated by various errors or noises, which can be represented in a simplified expression below:

$$\begin{aligned}\lambda_{1e} &= \int_0^t (V_1 - R_1 i_1)\, dt + \\ &\int_0^t (V_{1\varepsilon}(t) - R_{1\varepsilon}(t)\, i_1 - i_{1\varepsilon}(t)\, R_1)\, dt \\ &= \int_0^t (V_1 - R_1 i_1) dt + \int_0^t -(R_{1\varepsilon}(t) \cdot i_1) dt + \int_0^t (V_{1\varepsilon}(t) - i_{1\varepsilon}(t) R_1) dt \\ &= \lambda_1 + \lambda''_{i\varepsilon 0} + \lambda'_{1\varepsilon}\end{aligned} \tag{7}$$

where

$$\lambda_1 = \lambda_{1\alpha} + j\lambda_{1\beta},\ V_1 = V_{1\alpha} + jV_{1\beta}$$
$$i_1 = i_{1\alpha} + j i_{1\beta}$$

- $R_{1\varepsilon}t$: the value of motor stator resistance that deviates from its nominal value which is at room temperature or a calibrated value at a predetermined temperature.
- $V_{1\varepsilon}t$: includes the errors contributed by common-mode voltage and offset at motor terminals.
- $i_{1\varepsilon}t$: represents the total DC-offset and drifting terms in signal conditioning and processing circuitry of feedback currents.

- $\lambda'_{1\varepsilon}$: $\int_0^t -(R_{1\varepsilon}(t)\cdot i_1)dt$, the deviation contributed by the state resistance changes.

- $\lambda''_{1\varepsilon}$: $\int_0^t (V_{1\varepsilon}(t) - i_{1\varepsilon}(t)\cdot R_1)dt$, the error caused by the DC-offset and drifting of the signal processing circuit feed back primary current voltage.

For simplicity, the signal to noise ratio of the estimated motor flux can then be expressed by eqn (8):

$$S_{nr} = \frac{\int_0^t (V_1 - R_1 i_1)\,dt}{\int_0^t (V1\varepsilon\ (t) - R_{1\varepsilon}(t)\, i_1 - i_{1\varepsilon}(t)\, R_1\ )dt} \tag{8}$$

The magnitude of motor counter EMF is significantly low at low frequencies, i.e. below 2 Hz, and the voltage drop on stator resistor becomes a large proportion of the motor stator voltage. The thermal variation in R_1 is known to adversely affect the estimation of motor stator flux and a compensation method was detailed in [11]. However, this compensation can only address the second term of the denominator in eqn. 8, without affecting the first and the third items.

On the other hand, due to the small signal/noise ratio and integration effect as shown in eqn. 7 and 8, errors contributed from $V_{1\varepsilon}$t and $i_{1\varepsilon}$t actually accumulate. The error accumulation takes place via the integration effect of motor terminal variables. Once the accumulated error signal becomes significantly large in comparison with the real flux signal, it deteriorates the motor flux estimation. This in turn introduces error in the estimation of orientation angle, φ motor speed, ω_1, as well as the torque-producing current command, $i_{1\beta}$, at the output of speed regulator. The inaccuracy of the orientation angle directly affects the variable transformation between reference frames in both feed forward and feedback paths. As a result, more motor current distortion and torque oscillation can be observed.

Further experimental observation confirms that the control degradation takes place gradually and with an interactive loop effect. This can be analyzed from the point of view of error re-intrusion via feedback circuitry. The error re-intrusion and interaction with the control further corrupt the estimation and speed up the control degradation in this feedback system. As the process continues, a stable operation is difficult to maintain and the control system fails. Fig. 2 shows a motor current degradation from its initial healthy waveform at 2.5 Hz after about ten seconds of operation.

Observations above indicate that the stator resistance thermal variation is not the sole major problem that enchants encoderless control of induction machine at low frequency, although it has revealed a very important aspect

4.2 Control Information Starvation in Conventional Schemes when Speed Estimation Deteriorates

Following the technology evolution, many speed sensorless schemes employing speed estimation algori-thms to replace the speed encorders were developed as a natural extension of the field oriented control system. As a result, the top-level control structures or configurations look alike to each other and they experience similar problems at low frequency. It is necessary to have a brief review on the system topology and identify potential weakness.

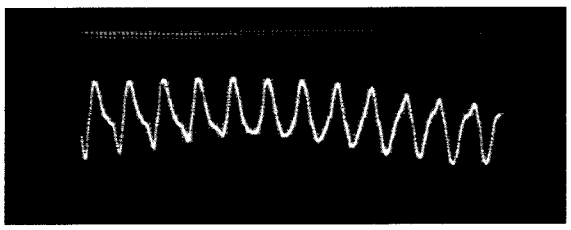

Phase current: 10 A/div , Time: 0.5 Sec/div

Fig. 2 Control degradation with motor current distortion when conventional algorithm is used

It is well known that most indirect field oriented control systems have explicit stator current feedback loops in a two-axis rotating reference frame. However, the machine flux control varies which can be cataloged into two groups (1) open loop structure. This is a reduced dimensional control of the motor flux vector. (2) Added amplitude control of the stator flux.

Conventional field orientation systems employ an inexplicit control scheme for the machine flux. In this topology, a predetermined reference profile of the flux producing current, i_{1d_ref}, is given by a microprocessor as an input to the i_{1d} inner loop to control the motor stator flux [4-5, 12]. This works when the machine parameters are accurately known and the field orientation system is tuned up. However, the machine flux regulation is more affected by the variation of the machine parameters that causes the detuned condition of the field orientation and nonlinearity such as machine magnetic saturation because there is no explicit feedback loop for the flux control.

An improvement can be obtained by adding a flux amplitude feedback loop into the basic scheme [11]. This scheme may be viewed as flux control in polar form in addition to the stator current control of i_{1d} and i_{1q} in a rectangular coordinate frame. The polar form configuration regulates the magnitude and the phase angle of

the stator or rotor flux to facilitate field orientation. The flux vector phase angle can be controlled by adjusting the angle ϕ of total rotor flux linkage λ_2 respecting to the stator datum as shown in Fig. 3. The output of the flux amplitude regulator produces the reference value of flux producing current for inner i_{1d} loop. This effectively maintains constant flux magnitude in steady state in the constant torque region. In field weakening region, it automatically reduces and corrects the reference value for the flux producing current. This makes it very suitable for deep field weakening operation. However, the drive control performance largely depends upon the accuracy of ϕ which is the function of the motor slip angular frequency and rotor electrical speed as given in eqn. 4 and 5.

The above review provides a foundation for further analysis of the control problem of speed sensorless AC drive at low speed. Due to loosing genuine speed estimation, the accuracy of the orientation angle ϕ, which is essential for flux vector control in the polar form, becomes uncertain as analyzed in section A. The control system runs into information starvation for motor flux orientation. The motor flux components cannot be controlled in the desired directions. A spiral vector diagram of the motor current and flux is illustrated in Fig. 3. The rotor flux components in this condition are given in eqn. (9) and (10).

As shown in Fig. 3 and eqns. (9) and (10), the decoupling control of the motor flux and torque is not available in this situation. The transient model of the induction machine degrades back to a fifth order and nonlinear plant. The polar form control of the machine flux vector breaks down. Therefore, a new control scheme at low frequency is necessary to regain the information and conditions for field orientation.

$$\lambda_{2d} = L_m i_{1d} + L_{22} i_{2d} \tag{9}$$

$$\lambda_{2q} = L_m i_{1q} + L_{22} i_{2q} \neq 0 \tag{10}$$

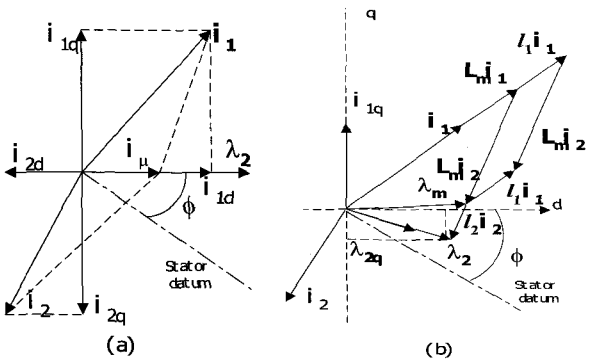

(a) Spiral vectors of induction motor current
(b) Spiral vectors of induction motor flux

Fig. 3 Motor current and flux relation in corrupted speed estimation at low speed

5. Proposed Scheme Of Speed Sensorless Control At Low Frequency

Proposed speed sensorless control scheme has two operation modes, one for low frequency and one for high frequency.

5.1 Speed Estimation and Control at Low Frequency

As analyzed above, because the estimated value of motor flux orientation angle in a speed-sensorless controlled AC drive is not accurate at low speed, it is desirable to replace the polar-form machine flux control by directly regulating two motor flux components of $_1$ that are perpendicular in rectangular form in a synchronous reference frame. In this way, we can explicitly control all four perpendicular components of the stator flux and current spiral vectors, λ_{1d}, λ_{1q}, i_{1d}, and i_{1q}, by their corresponding feedback loops, thus improving the performance of the control without a speed sensor. This approach can potentially resume a full-dimensional spiral vector control as will be highlighted below.

5.1.1 Full dimensional Spiral Vector Control Scheme

A simplified control block diagram of our new scheme is given in Fig. 4. The rotating angular speed of the reference frame can be estimated by a feed forward approach, which will be detailed in section A.2.

Because the accuracy of motor speed feeback based on the estimation is degraded at low frequency, the motor dynamic response and speed regulation must be achieved by an alternative approach. This approach is based on the fact that the motor no-load speed at a particular operating frequency is a close approximation of the motor synchronous speed. This is especially true at low frequency since the rotor windage loss is negligible. The motor load is then estimated by a closed-loop load observation based on a full dimensional motor vector control method. The load torque signal is then incorporated into the speed control to meet the speed regulation requirement.

In Fig. 4, both quadrature motor flux components are controlled in d and q axis of the synchronous rotating reference frame. The feedback stator flux components obtained from eqn. 1 and 2 are transformed into a synchronous reference frame by:

$$\begin{bmatrix} \lambda_{1d} \\ \lambda_{1q} \end{bmatrix} = \begin{bmatrix} \cos\varphi & \sin\varphi \\ -\sin\varphi & \cos\varphi \end{bmatrix} \begin{bmatrix} \lambda_{1\alpha} \\ \lambda_{1\beta} \end{bmatrix} \tag{11}$$

The control rules are set up such that all magnetization of the rotor is directed on to the d-axis and no magnetization is along the rotor q-axis as described by the following equations:

$$\lambda_{2d} = L_m i_{1d} + L_{22} i_{2d} \quad (12)$$

$$\lambda_{2q} = L_m i_{1q} + L_{22} i_{2q} = 0 \quad (13)$$

$$\lambda_{1q} = L_m / L_{22} \ \lambda_{2q} + L_{1\sigma} i_{1q} = L_{1\sigma} i_{1q} \quad (14)$$

Fig. 5 depicts the spiral vector diagram of motor currents and flux in its desired orientation of the induction motor control system without a speed sensor.

Flux control feedback loops in both d and q axes can be designed based on eqns. (11-14). When a sudden load applies onto the motor shaft, it slows down the rotor mechanical speed and increases the slip frequency of the induction machine. The total-rotor flux vector momentarily deviates from the d-axis of the rotating frame. The rotor q-axis flux component becomes non-zero and the state flux component becomes:

$$\lambda_{1q} = L_m / L_{22} \ \lambda_{2q} + L_{1\sigma} i_{1q} \quad (15)$$

A transient load signal can then be derived based on the variation of rotor q-axis flux component signal as a by-product of the quadrature flux regulation. In fact, based on eqns. (11)-(15), corresponding incremental changes in motor flux $\Delta\lambda_{2q}$ and $\Delta\lambda_{1q}$ can be detected and processed to increase the motor torque current. This in turn generates the corresponding electromagnetic torque to improve load rejection at transient state and achieve drive speed regulation in steady state.

$$\Delta T_e = K_T \Delta i_{1q} = K_L K_T L_m / L_{22} \ \Delta\lambda_{2q} \quad (16)$$

where K_L is the control coefficient.

To reduce common-mode noise and possible zero-sequence components in motor feedback voltage whose effect is indicated in eqn. (7) and (8), the voltage components in the two-axes frame are computed from the differential voltages at motor terminals instead of phase voltages. The matrix equation is given by eqn (17). This equation also allows a minimum circuit realization for three-phase motor voltage feedbacks because the third column of the coefficient matrix is zero.

$$\begin{bmatrix} V_{1\alpha} \\ V_{1\beta} \end{bmatrix} = \begin{bmatrix} 2/3 & 1/3 & 0 \\ 0 & -1/\sqrt{3} & 0 \end{bmatrix} \begin{bmatrix} V_{ab} \\ V_{bc} \\ V_{ca} \end{bmatrix} \quad (17)$$

To eliminate the DC-offset from the voltage integration circuits and the current feedback, DC-offset elimination algorithm, which consists of digital band-pass filtering with an adaptive bandwidth, is incorporated into the control system.

Finally, to improve the speed tracking performance to speed reference change at large signal, the motor speed is calculated from eqn. (18) and fedback to a speed regulator as shown in Fig. 4. This loop has a low bandwidth because heavy filtering is necessary.

$$\omega_{re} = \frac{(r_{1q} L_{1q}) i_{1q}}{V_{1q} - (\frac{L_m}{L_{22}} \lambda_2 + L_{1\sigma} i_{1d})} \quad (18)$$

where

$$r_{1q} = r_1 + \frac{L_{11}}{L_{22}} r_2 \ , \ L_{1q} = 2L_{1\sigma} , \ L_{1\sigma} = L_{11} - \frac{L_m^2}{L_{22}}$$

5.1.2 Feed forward approach producing unit- rotating vector

An alternative approach for the motor synchronous speed estimation other than the conventional method based on eqns. (1)-(3) is incorporated to reduce the accumulative error and loop reaction. The new approach is based on an understanding that the motor synchronous speed can be readily calculated from the inverter output fundamental frequency. The fundamental frequency of the inverter in kth sampling period of a microprocessor based discrete control system equals the frequency command value in the previous sampling period of (k-1). Therefore, in low frequency mode of Fig. 4, the frame orientation angle, φ, which is the angle of the d-axis of synchronous rotating reference frame with respect to the stator datum, is computed by directly integrating the commanded motor synchronous angular speed.

$$\varphi = \int_0^t \omega_1^* \, dt \quad (19)$$

The feedback errors associated with the low signal to noise ratio can be avoided.

5.2 Speed Estimation and Control at High Frequencies

At high speeds, a conventional speed estimation method can be employed because the signal/noise ratio associated with the sensing and integration of the stator back EMF becomes sufficiently benign at this region.

The estimation of the motor synchronous speed and the frame orientation angle can also be realized by using a phase-lock-loop approach [7]. The frame orientation angle, φ is then obtained by integration of the synchronous speed of the rotating reference frame according to eqn. 4.

The flux reference signals for a constant torque drive are calculated such that the airgap flux is maintained at a constant magnitude obtained when the machine is operated at its nameplate rating. A pre-calculated flux profile is incorporated for field weakening above a base frequency or when input line voltage is lower than its nominal value. Two operating modes, low speed and high speed, are eventually linked by a variable structure control to ensure a smooth transition.

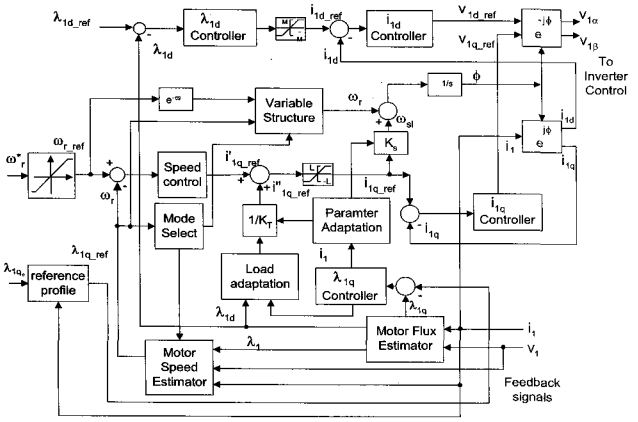

Fig. 4 Simplified block diagram of proposed speed sensorless control

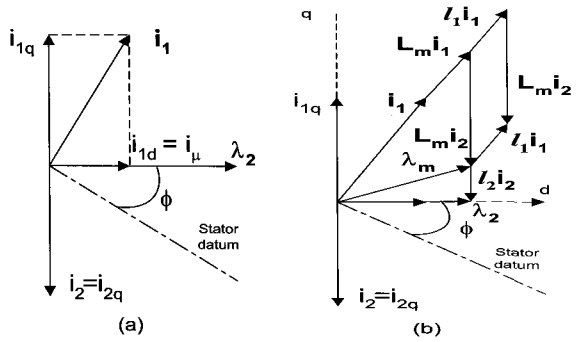

(a) Spiral vectors of induction motor current
(b) Spiral vectors of induction motor flux

Fig. 5 Motor current and flux in full dimensional flux vector control without a speed sensor

6. Experimental System Implementation and Result

A three-level inverter circuit is designed and implemented by using 1200 V and 100 A IGBTs. The maximum output voltage of the inverter is expected at 920 V. To observe the motor torque at low speed, a torque transducer is installed on a 15 Hp Motor-generator set. The nameplate data of the cage induction motor are given in Table 1. The control scheme is implemented in a DSP controller that is based on a low-cost single-chip DSP, TMS320C31. The DSP operates at 30 Mhz of clock frequency. The speed-sensorless control and three-level PWM control based on space-vector modulation algorithms have been implemented in C programming code. The program code and supporting modules are then compiled, linked and loaded into the DSP's memory for real execution. The space-vector modulation of three-level PWM control is reported in [11]. The DSP receives control reference commands, initial machine parameters, and system control parameters via a PC based RS232 communication link. The sampling frequency of the digital current control system is 1000 Hz for this three-level inverter system.

A drive speed response to a 67% step-load variation at 60 rpm (2 Hz at no-load) is shown in Fig. 6. The AC motor current responds very well to the step-load change by adjusting its amplitude, frequency and phase angle quickly to re-establish a torque balance at a new equilibrium point under the field oriented control. The control system possesses a good stability and performance in both transient and steady-state without a speed sensor. The three-phase motor currents are well controlled in a set of balanced sinusoidal waveforms.

An oscillogram of motor torque and speed response to a 67% step load application at 30 rpm (1 Hz at no-load) and 20 rpm (0.67 Hz at no-load) is shown in Fig. 7 and Fig. 8 respectively. The AC motor current is well under control with no DC-offset or distortion. The speed sensorless control system is capable of providing a transient electromagnetic torque in both small signal and large signal mode to balance the sudden impact load. The motor speed has a small transient drop as shown in Fig.s 7 and 8. However, a damped transient oscillation in the motor speed is observed when the load torque is removed as shown in the test results. The improved result will be incorporated in a later report.

The motor voltage and current waveforms of the 3-level inverter at high frequencies are satisfactory. The inverter switching frequency is only 500 Hz, which is selected to reduce the switching losses. The 3-L inverter and control have been reported in [11] and other literature. The drive control is stable over a wide speed range and capable of four-quadrant operations.

Table 1 Nameplate Data Of Test Induction Motor and Torque Transducer

Reliance RPM type, 15 HP, 21 A, 460 V, 60 Hz, 1770 RPM

r_1=0.34ohm	r_2=0.195ohm
l_1=0.0036H	l_2=0.0035H
L_m=0.1042H	J=0.4kg-m^2

Torque Transducer: Eaten, Elbow, Model 1104.

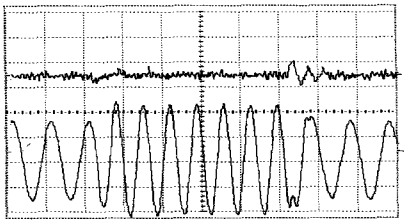

Trace 1: Motor speed.
Trace 2: Motor current: 20 A / div.
Time: 0.5 sec./div.

Fig. 6 Speed response to a 67% step-load variation at 60 rpm (no-load frequency: 2 Hz)

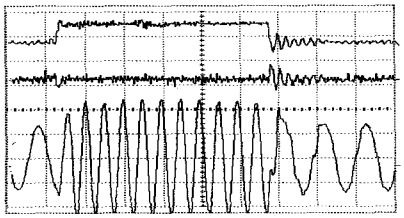

Trace 1: Motor torque, 40 FT-LB / div.
Trace 2: Motor speed
Trace 3: Motor current: 20 A / div.
Time: 1 sec./div.

Fig. 7 Speed response to a 67% step-load variation at 30 rpm (no-load frequency: 1 Hz)

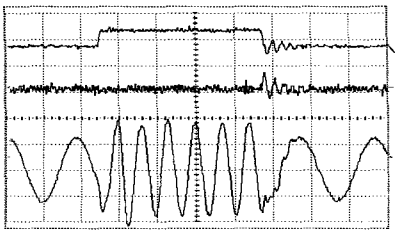

Trace 1: Motor torque, 40 FT-LB / div.
Trace 2. Motor speed
Trace 3: Motor current: 20 A / div.
Time: 1 sec./div.

Fig. 8 Speed response to a 67% step-load variation at 20 rpm (no-load frequency: 0.67 Hz)

7. Conclusions

The structural weakness in the conventional speed-sensorless control has been revealed. Main error sources in the estimation of induction motor flux and speed of a speed-sensorless drive are identified, and their negative impacts have been discussed. Analysis and experimental tests show that, in addition to the stator resistance variation, the accumulative errors over time from the integration of machine's voltage and current terms are largely responsible for the degradation of the estimation and control at low frequency region because the signal/noise ratio is very low. A loop-effect driven error amplification speeds up the degradation process as evidenced by our experiment shown in Fig. 2. A full-dimensional vector control scheme has been proposed and implemented. A novel control scheme is developed to improve the control performance of motor's current, torque and speed at low frequencies. Error reduction measures in both motor voltage and current feedback paths are also briefly discussed. The scheme resumes exercising of full dimensional vector control and is less sensitive to the combined effect of the error sources and loop effect in the low-frequency range. The system has been successfully implemented and tested based on a DSP controller with a 15 Hp induction machine fed by a 3-level IGBT inverter. Experimental results demonstrate that improved control for motor current, torque and speed is achievable even below 0.5 Hz.

Nomenclature

d, q: designate orthogonal axes in synchronous reference frame.
α, β:stationary two-axes reference frame.
L_{11}: $L_1 + l_1$.
L_{22}: $L_2 + l_2$.
L_1, L_2: stator and rotor airgap inductance.
l_1, l_2:stator and rotor leakage inductance.
L_m: stator-rotor mutual inductance.
λ_1,λ_2: stator and rotor flux linkage respectively.
$\lambda'_{1\varepsilon}$: deviation contributed by the state resistance changes.
$\lambda''_{1\varepsilon}$: error caused by the DC-offset and drifting of the signal processing circuit feedback primary current voltage.
ω_1: excitation radian frequency.
ω_{sl}: radian frequency of the rotor current.
p: differential operator, d/dt.
J: total inertia on the drive shaft.
f: drive friction coefficient.
T_e: electromagnetic torque of the motor.
T_L: load torque at the coupling of the motor.
ω_r,ω_{re}: rotor mechanical and electrical angular velocity.

References

[1] F. Blaschke, "A New Method for The Structure Decoupling of AC Induction Machines," 2nd IFAC on Multi-variable Tech. Control Systems, Pt 3, pp 11-13, Oct. 1971.

[2] R. Jotten and G. Maeder, "Control Methods for Good Dynamic Performance of Induction Motor Drives

Based on Current and Voltage As Measured Quantities," IEEE Trans. IAS Vol. IA-19, No. 3, 1983, pp. 356-363.

[3] A. Abbondanti and M. B. Brennen, "Variable Speed Induction Motor Drives Use Electronic Slip Calculator Based on Motor Voltage and Currents," IEEE Trans. IAS, Vol. IA-11, No. 5, 1975, pp. 483-488.

[4] T. M. Rowan, R.J. Kerkman, "A New Synchronous Current Regulator and an Analysis of Current-Regulated PWM Inverters," IEEE Trans. Ind. Appl., vol. 22, 1986, pp.678-690.

[5] L. Xu, R. D. Doncker and D. W. Novotny, "A Stator Flux Oriented Induction Machine Drive," PESC' 88 Conference Record, pp. 870 - 876.

[6] C. D. Schauder, "Adaptive Speed Identification for Vector Control of Induction Motors Without Rotational Transducers," 1989 IEEE IAS Conf. Record, pp. 491-499.

[7] X. Xu and D. W. Novotny, "Implementation of Direct Stator Flux Orientation Control on a Versatile DSP Based System," IEEE Trans. IAS, Vol. 27, No. 4, July/August 1991, pp. 694-700.

[8] H. Nakano and I. Takahashi, "Sensorless Field Oriented Control of An Induction Motor Using An Instantaneous Slip Frequency Estimation Method," 1988 IEEE PESC Record, pp. 847-854.

[9] J.C. Moreira, K.T. Hung, T.A. Lipo and R.D. Lorenz, "A Simple and Robust Adaptive Controller for Detuning Correction in Field Oriented Induction Machines," 1991 IEEE IAS Annual Meeting Conference, pp. 397-403.

[10] R.J. Kerkman, B.J. Seibel, T. M. Rowan and D. Schlegel, "A New Flux And Stator Resistor Identifier For AC Drive Systems," 1995 IEEE IAS Conf., pp. 310-318.

[11] Jie Zhang (Chang), "High Performance Control of A Three-Level IGBT Inverter Fed AC Drive," IEEE IAS Annual Meeting Conference Record, 1995, pp. 22-28.

[12] Jie Zhang (Chang) and T. H. Barton, "Microprocessor Based Primary Current Control for A Cage Induction Motor Drive," IEEE Trans. on Power Electronics, Vol. 4, No. 1, Jan. 1989, pp. 73-82.

Jie (Jay) Chang

He received the Ph.D. and M.Sc. degrees in electrical engineering from the University of Calgary, Calgary, Canada in 1985 and 1988, respectively He is the Associate Director of Florida Advanced Power Research Institute and Associate Professor at Florida State University. He was a Principal Scientist (equivalent to Senior Principal Engineer) and Manager of Department of Control & Power Technology at Rockwell's Corporate Research Center (RSC). Dr. Chang holds five U.S. patents and has published over 80 refereed technical papers in IEEE Transactions, international journals and major IEEE conferences. He has been an active IEEE Senior Member since 1992.